Supplementary Information for

Ultrafast Universal Quantum Control of a Quantum Dot Charge Qubit Using Landau-Zener-Stückelberg Interference

Gang Cao, Hai-Ou Li, Tao Tu, Li Wang, Cheng Zhou, Ming Xiao, Guang-Can Guo, Hong-Wen Jiang and Guo-Ping Guo

This PDF file includes:

Supplementary Figures. S1 to S3
Supplementary Discussion
Supplementary References

Supplementary Figures

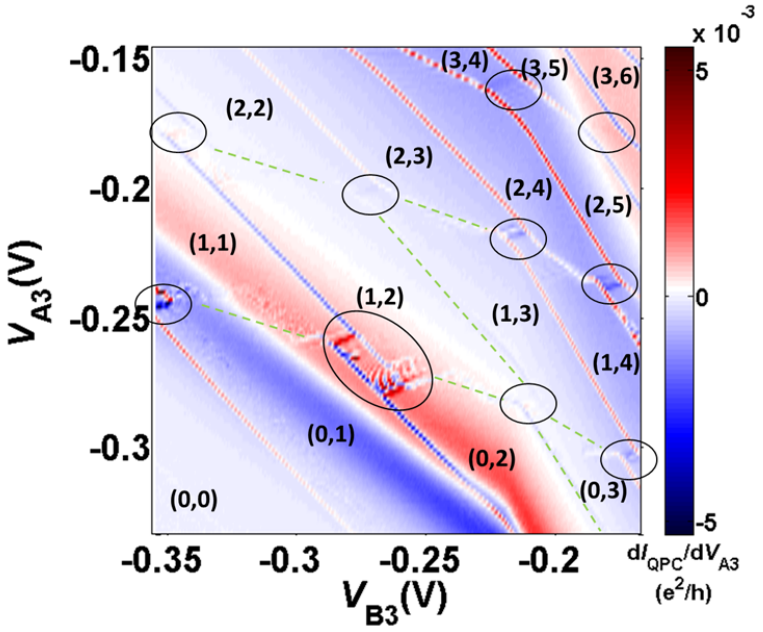

(a)

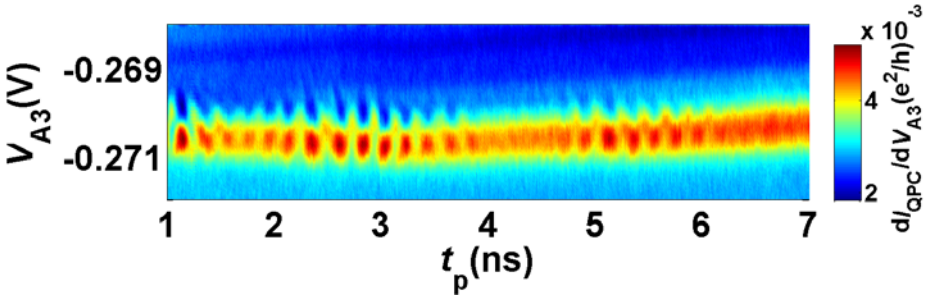

(b)

Supplementary Figure S1| Charge stability diagram of the double quantum dot and coherent oscillations of the charge qubit. (a) The QPC differential transconductance as a function of the gate voltages V_{A3} and V_{B3}. The notation (n,m) represents the effective left and right dot occupancy. The black ovals and green dashed lines indicate the various charge configurations. In the remainder of the paper, we focus on the regime denoted by the large oval. (b) The coherent oscillations of the qubit are exhibited in the QPC differential transconductance signal when a square-shaped non-adiabatic pulse of width t_p is applied. The anti-crossing energy gap 2Δ can be determined from the period of the coherent oscillations of the qubit between two charge states. Figure S1b shows a typical example of a period on the order of 200 ps.

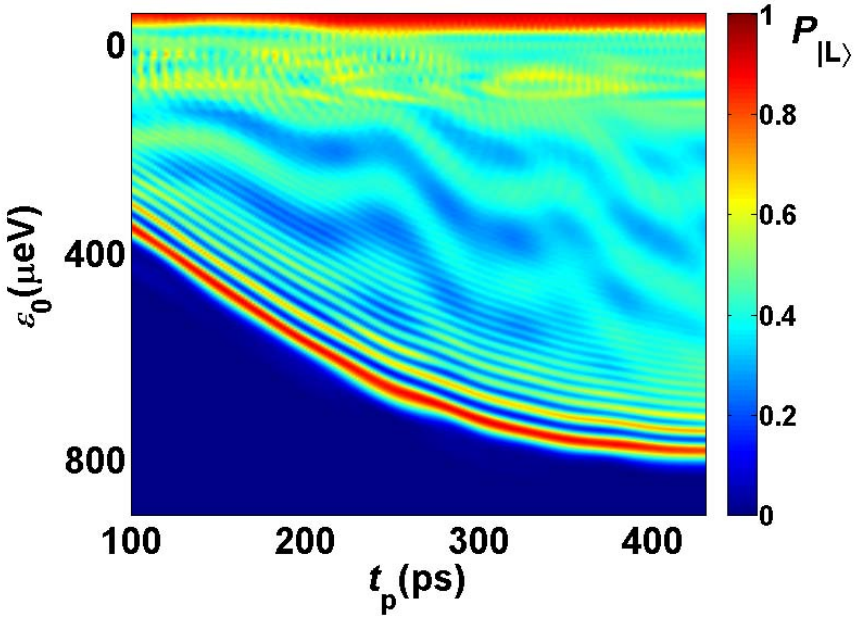

(a)

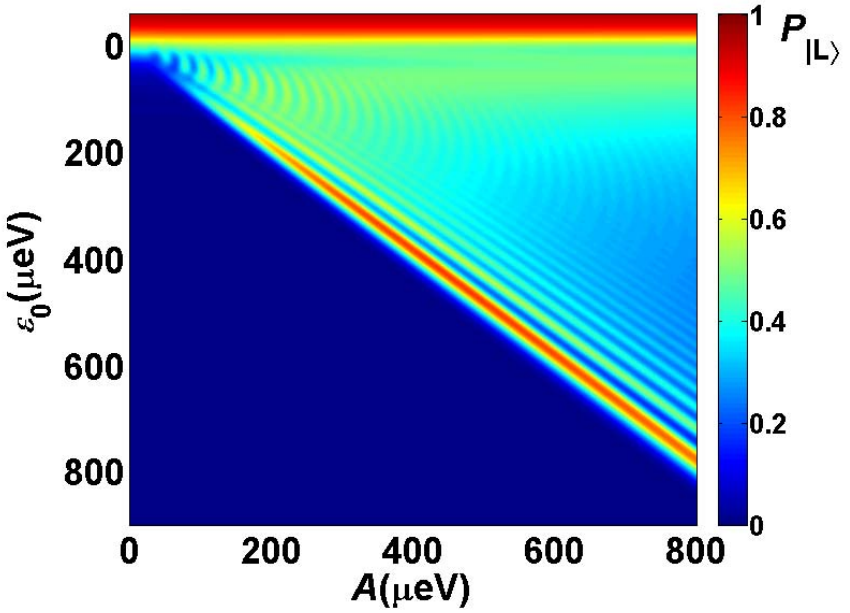

(b)

Supplementary Figure S2| Simulations of the qubit dynamics. Simulation results of the charge qubit probability $P_{|L\rangle}$ using the realistic pulse shape, which displays (a) coherent oscillations as a function of the detuning ϵ_0 and the pulse time t_p, and (b) the interference pattern as a function of the energy position ϵ_0 and the driven pulse amplitude A.

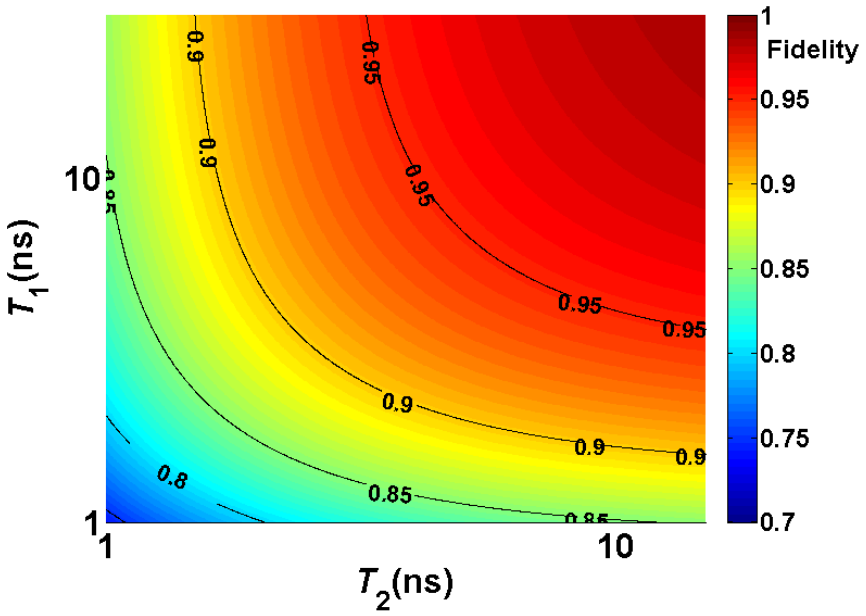

Supplementary Figure S3| Single qubit operation fidelity. Simulation results of the operation fidelity as a function of the pulse duration time t_p and the dephasing time T_2. The operation is a LZS pulse with an amplitude of 800 μeV.

Supplementary Discussion

(1) Charge Qubit and the Driven Pulse

The charge qubit in a double quantum dot is typically described by a Hamiltonian of a two-level system on the basis of $|\mathrm{L}\rangle$ and $|\mathrm{R}\rangle$, as follows [13,18]:

$$H = \frac{1}{2}\varepsilon(t)\sigma_{\mathrm{z}} + \Delta\sigma_{\mathrm{x}}.$$

The level detuning is $\varepsilon = E_{\mathrm{R}} - E_{\mathrm{L}}$, in which E_{L} and E_{R} are the energy levels for an electron in the left and right dots, respectively. The value Δ is the tunneling between the two dots, and σ_{x} and σ_{z} are the Pauli matrices. We denote the eigenstates of the above Hamiltonian as the ground and excited states $|0\rangle$ and $|1\rangle$ with the corresponding eigenvalues E_0 and E_1.

In practice, one thinks of Δ as being fixed by the system properties and ε as a control parameter[13,18]. Our detuning pulse for the quantum manipulation of the charge qubit is illustrated in Figure 2a of the main text.

(2) LZS interference as unitary operations

First, we define the single-qubit rotation operators as follows:

$$\mathrm{R}_{\mathrm{x}}(\theta) = \begin{pmatrix} \cos\frac{\theta}{2} & i\sin\frac{\theta}{2} \\ i\sin\frac{\theta}{2} & \cos\frac{\theta}{2} \end{pmatrix},$$

$$\mathrm{R}_{\mathrm{z}}(\phi) = \begin{pmatrix} \exp\left(\frac{-i\phi}{2}\right) & 0 \\ 0 & \exp\left(\frac{i\phi}{2}\right) \end{pmatrix},$$

on the basis of the ground and excited states $|0\rangle$ and $|1\rangle$.

In many previous experiments, the authors implemented periodic microwave diving field on the two-level system and observed the LZS interference (for an excellent review, please see Ref. [13], for a very recent example, please see Ref. [18]). Here we use an alternative method replacing microwave with a single pulse. The LZS interference process consists of three stages: (1) The system begins in the $|\mathrm{R}\rangle$ state and adiabatically evolves along the ground state $|0\rangle$ until the first LZ transition occurs at the anti-crossing point. The initial state becomes a coherent superposition of the ground and excited states, $|0\rangle$ and $|1\rangle$. (2) The two trajectories evolve

independently and accumulate a relative phase. (3) Upon return to the anti-crossing point, the second LZ transition occurs.

The effects of the passage through an anti-crossing point can be written as an unitary transformation[13,22,27-29]:

$$\mathrm{U_{LZ}} = \begin{pmatrix} \cos\frac{\theta_{\mathrm{LZ}}}{2}\exp(i\phi_{\mathrm{LZ}}) & i\sin\frac{\theta_{\mathrm{LZ}}}{2} \\ i\sin\frac{\theta_{\mathrm{LZ}}}{2} & \cos\frac{\theta_{\mathrm{LZ}}}{2}\exp(-i\phi_{\mathrm{LZ}}) \end{pmatrix}$$

in which the angle $\theta_{\mathrm{LZ}} = 2\sin^{-1}\sqrt{P_{\mathrm{LZ}}}$ depends on a Landau-Zener transition probability $P_{\mathrm{LZ}} = \exp(-2\pi\Delta^2/v\hbar)$, and v is the sweep velocity of the driving pulse through the anti-crossing point. The angle $\phi_{\mathrm{LZ}} = \phi_{\mathrm{s}} - \frac{\pi}{2}$ is related to the Stokes phase $\phi_{\mathrm{s}} = \frac{\pi}{4} + \arg\left[\Gamma\left(1 - i\frac{\Delta^2}{\hbar v}\right)\right] + \frac{\Delta^2}{\hbar v}\left(\ln\frac{\Delta^2}{\hbar v} - 1\right)$, and Γ is the Gamma function. Thus, the transformation can be presented, using the Euler angle decomposition, as a product of the form $\mathrm{U_{LZ}} = \mathrm{R_z}(-\phi_{\mathrm{LZ}})\mathrm{R_x}(\theta_{\mathrm{LZ}})\mathrm{R_z}(-\phi_{\mathrm{LZ}})$.

In the second stage, the qubit undergoes a single rotation about the z-axis (also called a phase-shift gate operation) $\mathrm{R_z}(\phi_{\mathrm{i}})$, in which ϕ_{i} is the phase accumulation.

In summary, the LZS interference can be treated as successive unitary operations as shown in Figure 2a of the main text:

$$\begin{aligned} |\Psi_{\mathrm{out}}\rangle &= \mathrm{U_{LZ}R_z}(\phi_{\mathrm{i}})\mathrm{U_{LZ}}|\Psi_{\mathrm{in}}\rangle \\ &= \mathrm{R_z}(-\phi_{\mathrm{LZ}})\mathrm{R_x}(\theta_{\mathrm{LZ}})\mathrm{R_z}(-\phi_{\mathrm{LZ}})\mathrm{R_z}(\phi_{\mathrm{i}})\mathrm{R_z}(-\phi_{\mathrm{LZ}})\mathrm{R_x}(\theta_{\mathrm{LZ}})\mathrm{R_z}(-\phi_{\mathrm{LZ}})|\Psi_{\mathrm{in}}\rangle \\ &= \mathrm{R}(\theta,\phi)|\Psi_{\mathrm{in}}\rangle. \end{aligned}$$

The above formula indicates that one can drive a two-level system from the state $|0\rangle$ to any desired state by controlling the speed of passage and the accumulated phase; essentially, an arbitrary one-qubit rotation $\mathrm{R}(\theta,\phi)$ can be realized.

(3) Phase accumulation in the LZS interference

Although the realistic pulse profile is Gaussian in this research, it is simply approximated as a triangular pulse. Using this approximation, one can obtain an analytic expression of the LZS interference that can be used to extract information from the experimental data. The pulse can be parameterized by the initial value of the detuning ε_0, the amplitude A, and the rise time t_{r}. One can easily obtain the time-dependent detuning as follows

$$\varepsilon(t) = \varepsilon_0 - vt, \qquad 0 < t < t_\mathrm{r},$$
$$\varepsilon(t) = \varepsilon_0 - A + v(t - t_\mathrm{r}), \qquad t_\mathrm{r} < t < 2t_\mathrm{r}.$$

The accumulated phase can then be calculated as

$$\phi_\mathrm{i} = \int_{t_0}^{t_\mathrm{r}} [E_1(t) - E_0(t)]dt + \int_{t_\mathrm{r}}^{2t_\mathrm{r}-t_0} [E_1(t) - E_0(t)]dt$$

in which $E_{1,0}(t) = \pm\sqrt{\varepsilon(t)^2 + (2\Delta)^2}$ represents the eigenvalues of the Hamiltonian of the system and t_0 is the time required to reach the anti-crossing point $\varepsilon = 0$. Substituting the explicit expression for $\varepsilon(t)$ into the above integral yields

$$\begin{aligned}\phi_\mathrm{i} &= 2\int_{t_0}^{t_\mathrm{r}} 2\sqrt{(\varepsilon_0 - vt)^2 + (2\Delta)^2}dt \\ &= 2\int_{0}^{t_\mathrm{r}-t_0} 2\sqrt{(vt)^2 + (2\Delta)^2}dt \\ &= 2v(t_\mathrm{r} - t_0)\sqrt{(t_\mathrm{r} - t_0)^2 + \left(\frac{2\Delta}{v}\right)^2} + 2\frac{(2\Delta)^2}{v}\ln\left|\frac{v(t_\mathrm{r} - t_0)}{2\Delta} + \sqrt{1 + \left(\frac{v(t_\mathrm{r} - t_0)}{2\Delta}\right)^2}\right|.\end{aligned}$$

Given that $t_\mathrm{r} = \frac{A}{v}$, and $t_0 = \frac{\varepsilon_0}{v}$, the following can be written:

$$\phi_\mathrm{i} = 2(A - \varepsilon_0)\sqrt{\left(\frac{A - \varepsilon_0}{v}\right)^2 + \left(\frac{2\Delta}{v}\right)^2} + 2\frac{(2\Delta)^2}{v}\ln\left|\frac{A - \varepsilon_0}{2\Delta} + \sqrt{1 + \left(\frac{A - \varepsilon_0}{2\Delta}\right)^2}\right|.$$

In our experiment, a short pulse ($\Delta/v \ll 1$) is applied; thus the above formula can be simplified to

$$\phi_\mathrm{i} = 2\frac{(A - \varepsilon_0)^2}{v}.$$

The total phase $\phi = \phi_\mathrm{i} - 2\phi_\mathrm{LZ} = 2\pi N$ gives rise to the constructive interference fringes. Neglecting a small contribution from $2\phi_\mathrm{LZ}$, we obtain the following for each interference node:

$$\phi = 2\frac{(A - \varepsilon_0)^2}{A}t_\mathrm{r}.$$

Rearranging the equation, we find the interference-node locations $\varepsilon_0^{(\mathrm{N})}$ as a function of the interference order N, $\varepsilon_0^{(\mathrm{N})} = A - \sqrt{2\pi\hbar AN/t_\mathrm{r}}$, which is the form we have used in Figure 2c of the main text.

(4) Determination of the total rotation angles in the LZS interference

Far from the anti-crossing point, the ground and excited states are roughly the charge eigenstates $|\mathrm{R}\rangle$ and $|\mathrm{L}\rangle$. Thus following the LZS interference, the project readout can be performed to measure the $|\mathrm{R}\rangle$ state for $|0\rangle$, and the $|\mathrm{L}\rangle$ state for $|1\rangle$, respectively.

Evaluating the successive operations starting from the $|0\rangle$ state,

$$|\Psi_{\mathrm{out}}\rangle = \mathrm{R_z}(-\phi_{\mathrm{LZ}})\mathrm{R_x}(\theta_{\mathrm{LZ}})\mathrm{R_z}(-\phi_{\mathrm{LZ}})\mathrm{R_z}(\phi_{\mathrm{i}})\mathrm{R_z}(-\phi_{\mathrm{LZ}})\mathrm{R_x}(\theta_{\mathrm{LZ}})\mathrm{R_z}(-\phi_{\mathrm{LZ}})|\Psi_{\mathrm{in}}\rangle,$$

we find that the final probability of reaching the $|\mathrm{L}\rangle$ state is as follows:

$$P_{|\mathrm{L}\rangle} = 2P_{\mathrm{LZ}}(1 - P_{\mathrm{LZ}})[1 + \cos(\phi_{\mathrm{i}} - 2\phi_{\mathrm{LZ}})].$$

The charge state probability $P_{|\mathrm{L}\rangle}$ is measured using the QPC sensor. To model the experimental results in Figure 3b, we include the decoherence time and a phenomenological term to account for pulse-induced damping effects[10].

One can easily observe that the measured $P_{|\mathrm{L}\rangle}$ exhibits clear oscillations as the total phase $\phi = \phi_{\mathrm{i}} - 2\phi_{\mathrm{LZ}} = 2\pi N$[13], which qualitatively confirms the experimental observations in the charge-stability diagram (Fig. 2b), the time domain (Fig. 4), and the pulse amplitude space (Fig. 3a) of the driven pulse in the main text.

As shown in Figure 2a of the main text, the total x- rotation is maximized when the z-rotations bring the Bloch vector back to the starting meridian of the Bloch sphere. Thus, at the positions under which the constructive interference occurs, we obtain the total rotation angles around the z- and x-axes as follows:

$$\begin{aligned}
\phi &= 2\frac{(A-\varepsilon_0)^2}{A}t_{\mathrm{r}}, \\
\theta &= 2\theta_{\mathrm{LZ}} \\
&= 4\sin^{-1}\left(\sqrt{P_{\mathrm{LZ}}}\right) \\
&= 4\sin^{-1}\left(\sqrt{\exp(-2\pi\Delta^2/\hbar v)}\right) \\
&= 4\sin^{-1}\left(\sqrt{\exp(-2\pi\Delta^2 t_{\mathrm{r}}/\hbar A)}\right).
\end{aligned}$$

Using the above two equations, we can fit the experiment data in Figure 3c and d of the main text to provide insights into the role of the control parameter A.

(5) Numerical simulations of the LZS interference

The time evolution of the charge qubit is given by solving the time-dependent master equations of the density matrix as follows:

$$\frac{d\rho}{dt} = -\frac{i}{\hbar}[\rho, H] + L,$$

In which H is the Hamiltonian introduced in Section 3. The standard Lindblad form L describes the incoherent process, including the appropriate relaxation and dephasing terms[30-32,11,9]. The solution of ρ involves a series of differential equations solved numerically using the Runge-Kutta method. The calculations shown in Figure S2 are in reasonable agreement with the experimental results (as compared with Figs. 4 and 3a of the main text).

(6) Operation fidelity of the LZS pulse

We can estimate the fidelity of each pulse-induced rotation on the Bloch sphere. The fidelity of a gate operation is defined as follows[30]:

$$F = \mathrm{Tr}\left[\sqrt{\rho_\mathrm{t}}\rho_\mathrm{e}\sqrt{\rho_\mathrm{t}}\right],$$

In which ρ_t is the density matrix of the desired target state and ρ_e is the density matrix of the real final state. In general, the fidelity is equal to the overlap between the ideal target state and the real final state after the control[30,33-35]. As previously explained, each LZS pulse-induced manipulation may be modeled as a rotation $\mathrm{R}(\theta, \phi)$ of the Bloch vector. From a comparison of the ideal predicted signal and the measured signal after a LZS-type operation, we can estimate a fidelity of 80% for a rotation of $\theta = 225^\circ$, and $\phi = 360^\circ$ (the second resonance in Fig. 3b in the main text).

Duration of a gate operation, the interactions of the charge states with their environment lead to a loss of fidelity[33,36-39]. Thus the fidelity depends on the specific properties of the environment and the parameters of the control pulse. As shown in Figure S3, we plot the fidelity of a specific operation pulse as a function of the pulse duration time and decoherence time. These results reveal that given an appropriate regime of charge-state decoherence, the value of the fidelity can be maintained above 90%. Further improvements can be expected from more advanced pulse-optimization methods[15,16], and fidelity values higher than 99% can be achieved.

(7) Decoherence time in a 2D Fourier transform of the amplitude spectroscopy

We use a different approach introduced by Rudner *et al.*[25] to determine the dynamics of a qubit in terms of two times: the intrinsic dephasing time T_2 and the ensemble-averaged dephasing T_2^*.

In an analogy to the interaction picture, we introduce a state vector as follows:

$$|\Psi(t)\rangle_{\mathrm{I}} = \exp(-i\varphi\sigma_{\mathrm{z}}/2)\,|\Psi(t)\rangle, \varphi = \int_0^t \varepsilon(t')dt'\,.$$

The new state evolves according to the Schrödinger equation $i\hbar\frac{\mathrm{d}|\Psi(t)\rangle_{\mathrm{I}}}{\mathrm{dt}} = H_{\mathrm{I}}|\Psi(t)\rangle_{\mathrm{I}}$ with the transformed Hamiltonian

$$H_{\mathrm{I}} = \frac{1}{2}\begin{pmatrix} 0 & \Delta^* \exp(-i\varphi\sigma_{\mathrm{z}}/2) \\ \Delta^* \exp(i\varphi\sigma_{\mathrm{z}}/2) & 0 \end{pmatrix}.$$

Next, we introduce the decoherence by including a correlated noise term $\varepsilon(t) + \delta\varepsilon(t)$ with the spectral density as follows:

$$S(\omega) = \frac{1}{2\pi}\int_{-\infty}^{+\infty} dt\,\exp(i\omega t)\,\langle\delta\varepsilon(t)\delta\varepsilon(0)\rangle_{\mathrm{ens}}\,.$$

If the system begins at the state $|\mathrm{R}\rangle$ and, the time evolution operator can be calculated in the first order of H_{I}

$$U(t) = 1 - \frac{i}{\hbar}\int_0^t H_{\mathrm{I}}(t')dt'\,.$$

Thus, we find the transition probability as follows:

$$\begin{aligned} P(t) &= \frac{1}{4}\left|-\frac{i}{\hbar}\int_0^t \Delta\,\exp\big(i\varphi(t')\big)\,dt'\right|^2 \\ &= \frac{1}{4\hbar^2}\int_0^t dt'\int_0^t dt''\Delta^2\exp\big[i\big(\tilde{\varphi}(t') - \tilde{\varphi}(t'')\big)\big]\exp\big[i\big(\delta\varphi(t') - \delta\varphi(t'')\big)\big]\,. \end{aligned}$$

We define the phases as

$$\varphi(t) = \tilde{\varphi}(t) + \delta\varphi(t), \tilde{\varphi}(t) = \int_0^t \varepsilon(t')dt'\,, \delta\varphi(t) = \int_0^t \delta\varepsilon(t')dt'\,.$$

Finally, we average over the noise realizations $\delta\varepsilon(t)$ to obtain

$$\langle P(t)\rangle_{\mathrm{ens}} = \frac{1}{4\hbar^2}\int_0^t dt'\int_0^t dt''\Delta^2\,\exp\big[i\big(\tilde{\varphi}(t') - \tilde{\varphi}(t'')\big)\big]\,\langle\exp\big[i\big(\delta\varphi(t') - \delta\varphi(t'')\big)\big]\rangle_{\mathrm{ens}}.$$

For the white noise model, we have

$$\langle\exp\big[i\big(\delta\varphi(t') - \delta\varphi(t'')\big)\big]\rangle_{\mathrm{ens}} = \exp[-\Gamma|t'' - t'|]\,.$$

Thus the decay law of the qubit is characterized by the rate Γ, which corresponds to the intrinsic dephasing time $T_2 = 1/\Gamma$.

In more general situations, the dephasing also occurs for a single two-level system in the time-ensemble measurement due to the low frequency noise, similar to the NMR averaging over

spin ensembles due to spatial inhomogeneities. We consider a Gaussian-distributed noise which yields the following:

$$\langle \exp\left[i\left(\delta\varphi(t') - \delta\varphi(t'')\right)\right]\rangle_{\mathrm{ens}} = \exp\left[-\frac{t^2}{2}\int_{-\infty}^{+\infty} d\omega S(\omega)\frac{\sin^2(\omega t/2)}{(\omega t/2)^2}\right] = \exp\left[-\frac{1}{2}t^2\Gamma^{*2}\right].$$

The rate $\Gamma^* = 1/T_2^*$ is introduced as the root-mean-square amplitude of the noise. Thus, the decay law is replaced by a function that contains the ensemble-averaged dephasing time T_2^*.

Usually, the ensemble-averaged and intrinsic dephasing processes can be distinguished using Ramsey and echo experiments, respectively. However, we demonstrate their differences using the 2D Fourier transform of the LZS interference pattern.

With the Fourier transformation

$$P_{\mathrm{FT}}(k_\varepsilon, k_{\mathrm{A}}) = \int_{-\infty}^{+\infty}\int_{-\infty}^{+\infty} \exp(-iAk_{\mathrm{A}} - i\varepsilon k_\varepsilon)\, P(\varepsilon, A) d\varepsilon dA\,,$$

we can conveniently repeat the calculation in Ref. [25] and find that the prefactor $\exp[-\Gamma|t'' - t'|/2]$ in the time domain leads to the corresponding prefactor in the amplitude domain

$$P_{\mathrm{FT}}(k_\varepsilon, k_{\mathrm{A}})_{\mathrm{i}} \propto \exp(-\Gamma k_\varepsilon).$$

Similarly, the ensemble-averaged Fourier transformation can yield the following:

$$P_{\mathrm{FT}}(k_\varepsilon, k_{\mathrm{A}})_{\mathrm{e}} \propto \exp\left(-\frac{1}{2}\Gamma^{*2}k_\varepsilon^2\right).$$

Obviously, the Fourier intensity with intrinsic dephasing corresponds to a linear relationship, while that with ensemble-averaged dephasing corresponds to a parabolic relationship. Hence, the 2D Fourier transformation has the great advantage of providing an effective way to distinguish between the types of dephasing time (as shown in Fig. 5 of the main text).

Supplementary References

27. Ashhab, S., Johansson, J. R., Zagoskin, A. M., and Nori, F. Two-level system driven by large-amplitude fields. *Phys. Rev. A* **75**, 063414 (2007).

28. Kayanuma, Y. Stokes phase and geometrical phase in a driven two-level system. *Phys. Rev. A* **70**, R2495 (1997).

29. Sillanpaa, M., Lehtinen, T., Paila, A., Makhlin, Y. and Hakonen, P. Continuous-time monitoring of Landu-Zener interference in a Cooper-pair box. *Phys. Rev. Lett.* **96**, 187002 (2006).

30. Nielsen, M. A. and Chuang, I. L. *Quantum computation and quantum information*. (Cambridge Univ. Press, 2000).

31. Xu, X., Sun, B., Berman, P. R., Steel, D. G., Bracker, A. S., Gammon, D. and Sham, L. J. Coherent optical spectroscopy of a strongly driven quantum dot, *Science* **317**, 929-932 (2007).

32. Fu, K. C., Clark, S. M., Santori, C., Stanley, C. R., Holland, M. C. and Yamamoto, Y. Ultrafast control of donor-bound electron spins with single detuned optical pulses. *Nature Physics* **4**, 780-784 (2008).

33. Piermarocchi, C., Chen, P., Dale, Y. S. and Sham, L. J. Theory of fast quantum control of exciton dynamics in semiconductor quantum dots. *Phys. Rev. B* **65**, 075307 (2002).

34. Li, X., Wu, Y., Steel, D., Gammon, D., Stievater, T. H., Katzer, D. S., Park, D., Piermarocchi, C. and Sham, L. J. An all-optical quantum gate in a semiconductor quantum dot. *Science* **301**, 809-811 (2003).

35. Economou, S. E., Sham, L. J., Wu, Y. and Steel, D. G. Proposal for optical U(1) rotations of electron spin trapped in a quantum dot. *Phys. Rev. B* **74**, 205415 (2006).

36. Rabl, P., Kolkowitz, S. J., Koppens, F. H. L., Harris, J. G. E., Zoller, P. and Lukin, M. D. A quantum spin transducer based on nanoelectromechanical resonator arrays. *Nature Physics* **6**, 602-608 (2010).

37. Yao, N. Y., Jiang, L., Gorshkov, A. V., Maurer, P. C., Giedke, G., Cirac, J. I. and Lukin, M. D. Scalable architecture for a room temperature solid-state quantum information processor. *Nature Communications* **3**, 800 (2012).

38. Emary, C., Xu, X., Steel, D. G., Saikin, S. and Sham, L. J. Fast initialization of the spin state of an electron in a quantum dot in the Voigt configuration. *Phys. Rev. Lett.* **98**, 047401 (2007).

39. Chen, L., Sham, L. J. and Waks, E. Optically controlled phase gate for two spin qubits in coupled quantum dots. *Phys. Rev. B* **85**, 115319 (2012).